Bioconjugate Chemistry

Article

pubs.acs.org/bc

# Enzyme-Catalyzed Conversion of Chemical Structures on the Surface of Gold Nanorods

Eriko Kusaka, Takeo Ito,* Kazuhito Tanabe, and Sei-ichi Nishimoto

Department of Energy and Hydrocarbon Chemistry, Graduate School of Engineering, Kyoto University, Nishikyo-ku, Kyoto 615-8510, Japan

Supporting Information

**ABSTRACT:** For developing metal nanoparticles of which surface chemical structures could be altered by enzymes in the cells, functional linkers caged by coumaric acids have been synthesized. Synthesized gold nanorod (GNR) conjugates possessing coumaric acid precursors underwent (porcine liver) esterase-catalyzed hydrolysis on their surface to afford GNRs coated with amino-functionalized polyethylene glycol and fluorescent coumarins as reporter molecules for monitoring the conversion. The chemical structural conversion on the GNR surfaces was successfully observed inside cells by fluorescence microscopy when GNR conjugates were incubated with tumor cells.

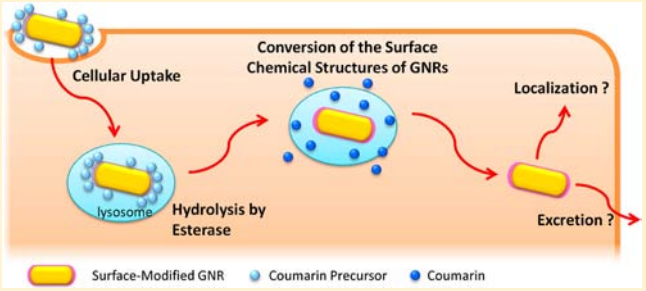


## INTRODUCTION

Recent progress in nanoscience and technology is providing great impetus for the development of new functional nanomaterials that display physical and chemical properties that are quite different from those of their bulk counterparts. In particular, organic and inorganic nanoparticles have attracted much interest from the viewpoint of biological applications such as tools for bioimaging, diagnostics, and tissue- and cell-specific drug delivery.[1−10]

Previous *in vitro* studies have demonstrated that synthetic nanoparticles can be incorporated into living cells depending on their size, shape, surface charge, and surface chemistry, mainly via the endocytic pathway. It is thus important to explore the effects of the surface properties of nanoparticles on the possible interactions between nanoparticles and biomolecules, such as lipids and proteins that compose intracellular structures, to understand the mechanisms of cellular uptake and the following clearance from the cells. For example, as evaluated by *in vitro* cytotoxicity assays, most engineered gold nanoparticles are found to be less toxic or nontoxic toward cultured cells.[11−14] However, some reports indicated that the cytotoxic effects are dependent on the surface properties of gold nanoparticles, possibly because interactions between nanoparticles and biomolecules (such as lipids or proteins) could lead to the destruction of biological processes in cells.[15−18] Positively charged nanoparticles are generally taken up well into the cells by electrostatic interaction because of the negatively charged lipids of the plasma membrane.[13,19−24] Despite the repellent interaction between negatively charged nanoparticles and the cell membrane, some nanoparticles that carry negatively charged functional groups on the surface can be taken up into the cells.[24−26] One of the major internalization pathways of nanoparticles is endocytosis. Nanoparticles present in the extracellular fluid or deposited on the plasma membrane are enclosed in vesicles of lipids and delivered to the endosomal compartment, following the endosomes merging with lysosomes. In the lysosomal compartments the nanoparticles are exposed to hydrolases capable of degrading organic molecules. Cellular uptake, however, is not the only factor determining intracellular concentration of nanoparticles: the relative abilities of the host cells to remove the nanoparticles also decide their ultimate fate. Although understanding the ensuing processes, such as localization in the organelles and excretion from the cells, is important for modulating cellular processes of the engineered nanoparticles and for identifying their cytotoxic effects,[27] quantitative studies on their mechanisms are still challenging.[28−31] Especially, the effects of the surface charge and chemical structure of nanoparticles on their excretion from the host cells are not yet well explored. It has been reported that engineered nanoparticles trap extracellular biomolecules such as proteins on their surfaces depending on the chemical structures and change their surface properties.[15−18] Therefore, molecular tools for determining surface properties of the nanoparticles inside the cells would be useful for investigating the intracellular processing mechanisms.

Here we report the development of metal nanoparticles possessing functional linkers protected by esterase-sensitive coumaric acids that can be enzymatically hydrolyzed to afford functional groups on the surface of nanoparticles and, at the same time, to form fluorescent coumarins as reporter molecules

**Received:** October 11, 2012
**Revised:** July 23, 2013
**Published:** July 27, 2013





dx.doi.org/10.1021/bc3005599 | *Bioconjugate Chem.* 2013, 24, 1435−1444

of the conversion process (Figure 1). Because of the "masking" effect of the protecting group, the variation in surface chemical

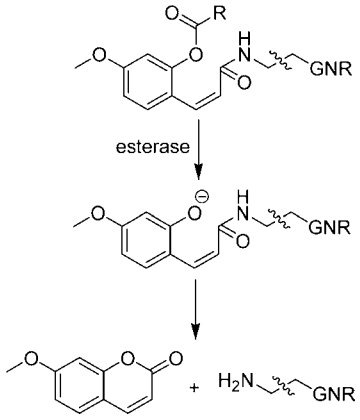


**Figure 1.** Esterase-catalyzed formation of GNRs possessing amino linkers on the surface.

structures induces minimal effects on the internalization process, but once the nanoparticles are taken up, esterase-catalyzed hydrolysis induces structural conversion of the surface linkers. Coumarin-based prodrug strategies were originally developed by Wang's groups,[32−35] and similar prodrugs possessing a "trimethyl lock"[36−39] have been successfully applied to drug delivery systems. In the present study, we developed esterase-sensitive surface modifiers possessing coumaric acid structures, which are applicable for understanding and modulating interaction between surface-modified nanoparticles and biomolecules inside living cells. The coumaric acid protecting groups at the termini of the surface linkers enable estimation of the relative efficiency of the structural conversion into the terminal amino groups on the surface based on the fluorescence intensity of the released coumarin by using high throughput fluorescence microplate readers. The coumarin-forming precursors are almost non-fluorescent, and thus a high signal-to-noise ratio is expected in the present system, which is an advantage over the fluorescence-quenching-based fluorophore−metal nanoparticle conjugates, in which quenching efficiency usually depends on the distance between the fluorophores and the nanoparticles.[22,40−42]

We synthesized gold nanorods (GNRs) with amino-functional linkers protected by coumaric acids. We then successfully quantified esterase-catalyzed conversion of the surface chemical structures in living cells by monitoring fluorescence from the generated coumarins. This approach can be applied for quantitative evaluation of the surface structure conversion and the subsequent alteration of the intracellular dynamics of metal nanoparticles for designing new drug delivery nanocarriers.

## EXPERIMENTAL PROCEDURES

**General Methods.** Reagents were purchased from commercial sources and were used without further purification. Preparative HPLC was performed with a Tosoh LC system (DP-8020 pumps, UV-8011 detector, AS-8020 auto sampler, and FC-8000 fraction collector) equipped with a reversed-phase column (5 $\mu$m, $\phi$10 × 250 mm, Inertsil ODS-3, GL Sciences). Analytical HPLC was carried out with a Shimadzu 10A HPLC system. Sample solutions were injected onto a reversed-phase column (5 $\mu$m, $\phi$4.6 × 250 mm, Inertsil ODS-3). The mobile phase containing acetonitrile was buffered with formic acid or acetic acid and delivered at a flow rate of 0.6 mL $min^{-1}$. The eluents were monitored by UV absorbance at 310 nm. $^1H$ and $^{13}C$ NMR spectra were recorded on a JEOL JNM-AL 300, a JEOL EX 400, or a JEOL GSX 270 spectrometer. The chemical shifts were expressed in ppm downfield from the signals of solvents as internal standards. Fast atom bombardment (FAB) mass spectrometry was recorded on a JMS-SX102A (JEOL) mass spectrometer, using 3-nitrobenzyl alcohol or polyethylene glycol (PEG) as a matrix. Electrospray ionization mass spectrometry was carried out with a Bruker Daltonics micro time-of-flight spectrometer. Fluorescence spectra were obtained on a Shimadzu RF-5300PC spectrofluorophotometer. UV−visible absorption spectra were measured with a JASCO V-530 UV/vis spectrophotometer.

**Organic Synthesis.** *Ethyl 3-(2-Hydroxy-4-methoxyphenyl)-(E)-2-propenoate (**1**).*[43,44] A mixture of 2-hydroxy-4-methoxybenzaldehyde (1.08 g, 7.1 mmol) and ethyl-(triphenylphosphoranylidene) acetate (5.03 g, 14.5 mmol) in 30 mL of $CH_2Cl_2$ was stirred at ambient temperature for 30 min. The mixture was washed with brine, dried over $MgSO_4$, and then concentrated under reduced pressure. Column chromatography (30−50% EtOAc/hexanes) of the residue gave the desired product **1** (1.62 g, quant.).

*3-(2-Isobutyryloxy-4-methoxyphenyl)-(E)-2-propenoic Acid (**3**).* A solution of the ethyl ester **1** (1.40 g, 6.3 mmol) in ethanol (30 mL), 5 M NaOH (2.5 mL), and water (30 mL) was refluxed under an $N_2$ atmosphere for 6 h. The dark solution was cooled to room temperature and 6 M HCl was added until the solution became acidic and a white precipitate appeared. The solid was filtered, washed with $CH_2Cl_2$, and then dried under reduced pressure. Carboxylic acid **2** (1.07 g, 88%) was obtained as a white solid and used without further purification. To a solution of **2** (499 mg) in dry THF (35 mL) was added dropwise isobutyric anhydride (557 mg, 3.5 mmol), then triethylamine (645 mg, 6.5 mmol) and 4-dimethylaminopyridine (DMAP; 64 mg, 0.52 mmol) under an $N_2$ atmosphere at 0 °C. After 10 min stirring at 0 °C, the solution was further stirred at ambient temperature for 2 h. The resulting solution was washed with water and then with diluted aqueous HCl (pH ∼4). The organic layer was dried over $MgSO_4$ and filtered, and the solvent was removed under reduced pressure. Column chromatography (2% MeOH/$CHCl_3$ + 1% $CH_3COOH$) gave the desired product **3** as a white solid (661 mg, 96%): $^1H$ NMR (400 MHz, $CDCl_3$) $\delta$ 7.66 (d, $J$ = 8.8 Hz, 1H), 7.64 (d, $J$ = 16.1 Hz, 1H), 6.85 (dd, $J$ = 2.4, 8.9 Hz, 1H), 6.66 (d, $J$ = 2.4 Hz, 1H), 6.33 (d, $J$ = 16.1, 1H), 3.80 (s, 3H), 2.89 (m, 1H), 1.34 (d, $J$ = 7.0 Hz, 6H); $^{13}C$ NMR (100 MHz, $CDCl_3$) $\delta$ 176.8, 170.3, 163.7, 152.2, 139.1, 129.5, 120.9, 118.6, 113.8, 109.4, 56.2, 35.3, 19.3; HRMS (FAB+) $m/z$: Calcd for $C_{14}H_{17}O_5^+$: 265.1076 $[M+H]^+$, found 265.1071 $[M+H]^+$.

*3-(2-Isobutyryloxy-4-methoxyphenyl)-(Z)-2-propenoic Acid (**3′**).* An acetonitrile solution (15 mL) of the *trans* isomer **3** (52 mg, 0.2 mmol) in a quartz glass vial was exposed to UV light (312 nm) from an FTI-20L transilluminator (Funakoshi) at ambient temperature for 30 min. The solution was diluted with ion-exchanged water (10 mL) and purified by HPLC using 35% acetonitrile/water containing 0.1% formic acid (3 mL/min) as a mobile phase and the desired product was eluted at 46 min after the injection. Lyophilization of the isolated fractions gave the *cis* isomer **3′** as a white solid (17 mg, 32%): $^1H$ NMR (400 MHz, $CDCl_3$) $\delta$ 7.60 (d, $J$ = 8.6 Hz, 1H), 6.83 (d, $J$ = 12.4 Hz, 1H), 6.73 (dd, $J$ = 2.2, 8.6 Hz, 1H), 6.57 (d, $J$ =


dx.doi.org/10.1021/bc3005599 | Bioconjugate Chem. 2013, 24, 1435−1444

2.4 Hz, 1H), 5.93 (d, $J$ = 12.2, 1H), 3.78 (s, 3H), 2.78 (m, 1H), 1.28 (d, $J$ = 6.8 Hz, 6H); $^{13}$C NMR (100 MHz, $CDCl_3$) $\delta$ 175.1, 170.3, 161.0, 149.6, 137.5, 131.6, 120.8, 120.4, 111.5, 107.5, 55.5, 34.1, 18.9; HRMS (FAB+) $m/z$: Calcd for $C_{14}H_{17}O_5^+$: 265.1076 $[M+H]^+$. Found 265.1078 $[M+H]^+$.

*Ethyl (E)-3-(8-Hydroxyjulolidine-9-yl)-2-methylpropenate (**4**).* Ethyl ester **4** was synthesized following the previously reported procedure.[45] A solution of 8-hydroxyjulolidine-9-carboxaldehyde (435 mg, Tokyo Chemical Industry) and [1-(ethoxycarbonyl)ethylidene]triphenylphosphorane (1.45 g, Wako) in $CH_2Cl_2$ (5 mL) was stirred at 40 °C under an $N_2$ atmosphere for 22 h. The resulting solution was cooled to room temperature and dried under reduced pressure. The crude product was purified by column chromatography (0–25% EtOAc/hexanes) to afford **4** as a yellow solid (521 mg, 87%).

*(E)-3-(8-Hydroxyjulolidine-9-yl)-2-methylpropenoic Acid (**5**).*[45] A solution of ester **4** (401 mg) in ethanol (3 mL), 5 M NaOH (2 mL), and water (5 mL) was refluxed under a $N_2$ atmosphere for 2 h. The solution was cooled to room temperature and acidified with 6 M HCl. The resulting mixture was extracted with $CHCl_3$ and the organic layer was dried over $Na_2SO_4$, filtered, and then dried under reduced pressure. Column chromatography (0–4% MeOH/$CHCl_3$) gave the desired product **5** as a green solid (294 mg, 81%).

*(E)-3-(8-Isobutyryloxyjulolidine-9-yl)-2-methylpropenoic Acid (**6**).* To the carboxylic acid **5** (294 mg) in dry $CH_2Cl_2$ (6 mL) were added isobutyric anhydride (216 $\mu$L), DMAP (26 mg), and triethylamine (265 $\mu$L) under an $N_2$ atmosphere, and the solution was stirred at ambient temperature under an $N_2$ atmosphere for 2 h. The resulting solution was washed with water and then with diluted aqueous HCl (pH ~4). The organic layer was dried over $MgSO_4$, filtered, and then evaporated under reduced pressure. Column chromatography (0–1% MeOH/$CHCl_3$) gave the desired product **6** with a small amount of isobutyric acid. For NMR measurement, the mixture was further purified by HPLC to give **6** as a yellow solid (276 mg, 75%): $^1$H NMR (400 MHz, $CDCl_3$) $\delta$ 7.62 (s, 1H), 6.97 (s, 1H), 3.19–3.13 (m, 4H), 2.84–2.80 (m, 1H), 2.72 (t, $J$ = 6.2 Hz, 2H), 2.50 (br, s, 2H), 2.07 (s, 3H), 1.96–1.89 (m, 4H), 1.33 (d, 6H); $^{13}$C NMR (100 MHz, $CDCl_3$) $\delta$ 174.8, 174.0, 146.6, 144.5, 135.5, 127.9, 123.7, 118.2, 115.1, 113.3, 49.8, 49.2, 34.3, 27.6, 21.7, 21.4, 21.0, 19.1, 13.9; HRMS (FAB+) $m/z$: Calcd for $C_{20}H_{26}NO_4^+$: 344.1856 $[M+H]^+$, found 344.1873 $[M+H]^+$.

*(Z)-3-(8-Isobutyryloxyjulolidine-9-yl)-2-methylpropenoic Acid (**6′**).* An acetonitrile solution (20 mL) of the *trans* isomer **6** (52.4 mg, 0.15 mmol) in a quartz glass vial was exposed to UV light (365 nm) at 4 °C for 45 min. The solution was diluted with water (6 mL) and methanol (8 mL), and then subjected to HPLC purification (mobile phase: 70% acetonitrile/10 mM triethylamine–acetic acid buffer (pH 7.0), 3 mL/min). Desired product was eluted at 8–9 min after the injection. Lyophilization of the isolated fractions gave the *cis* isomer **6′** as a white solid (12.6 mg, 24%): $^1$H NMR (400 MHz, $CDCl_3$) $\delta$ 6.73 (s, 1H), 6.46 (s, 1H), 3.13–3.09 (m, 4H), 2.83–2.81 (m, 1H), 2.67 (t, $J$ = 6.4 Hz, 2H), 2.51 (s, br, 2H), 2.02 (d, $J$ = 1.9 Hz, 3H), 1.94–1.91 (m, 4H), 1.30 (d, $J$ = 6.9 Hz, 6H); $^{13}$C NMR (100 MHz, $CDCl_3$) $\delta$ 176.7, 170.9, 144.3, 144.1, 132.4, 129.4, 127.4, 119.3, 116.2, 112.7, 49.8, 49.1, 34.3, 27.2, 21.7, 21.3, 21.1, 20.9, 8.8; HRMS (FAB+) $m/z$: Calcd for $C_{20}H_{25}NO_4$: 343.1784 $[M]^+$, found 343.1784 $[M]^+$.

*2,3,6,7-Tetrahydro-10-dimethyl-1H,5H,11H-[1]-benzopyrano[6,7,8-ij]quinolizin-11-one (**7**).* To a solution of ethyl ester **4** (34.5 mg, 0.11 mmol) in ethanol (5 mL) was added 0.1 M $NaHCO_3$ (0.5 mL). The yellow solution in a quartz glass vial was exposed to UV light (365 nm) from a transilluminator at ambient temperature for 1 h. The resulting fluorescent solution was evaporated under reduced pressure, resuspended in water, and then extracted with $CHCl_3$. The organic layer was dried over $MgSO_4$, filtered, and evaporated under reduced pressure. A yellow solid was obtained as the desired coumarin **7** (28.1 mg, 0.1 mmol, 90%): $^1$H NMR (400 MHz, $CDCl_3$) $\delta$ 7.19 (s, 1H), 6.70 (s, 1H), 3.17–3.13 (m, 4H), 2.80 (t, 2H, $J$ = 6.46 Hz), 2.67 (t, 2H, $J$ = 6.34 Hz), 2.04 (s, 3H), 1.92–1.85 (m, 4H); $^{13}$C NMR (100 MHz, $CDCl_3$) $\delta$ 163.6, 150.8, 144.8, 140.3, 124.0, 118.2, 117.5, 108.9, 106.6, 49.9, 49.6, 27.4, 21.6, 20.7, 20.4, 16.7; HRMS (FAB+) $m/z$: Calcd for $C_{16}H_{18}NO_2$: 256.1338 $[M+H]^+$, found 256.1342 $[M+H]^+$.

*Amino Linkers.* Bifunctional PEG linkers possessing amino and thiol groups on their termini (**L2** and **L4**) were purchased from Dojindo Laboratories and JenKem Technology USA, respectively (Figure 2). Amino-PEG-thiol **L3** was synthesized

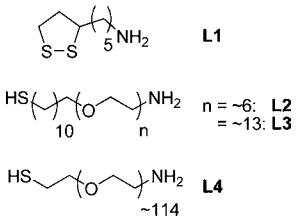


**Figure 2.** Chemical structures of the amino linkers (**L1**–**4**).

according to the synthetic procedure reported by Fiammengo's group.[46] 1,2-Dithia-3-(1-amino-*n*-pentyl)cyclopentane (**L1**) was synthesized following the previously reported procedure[47] with a slight modification. DL-$\alpha$-Lipoamide (1.0 g) was dissolved in 30 mL of dry THF. The solution was added to $BH_3$–THF (2.5 equiv, Nacalai) at ambient temperature. After 30 min stirring, the mixture was further refluxed under an $N_2$ atmosphere for 24 h. The mixture was cooled to room temperature, and 6 M HCl (5 mL) was added to the mixture. The mixture was again refluxed for 1 h, and then the pH of the solution was adjusted to 6–7 with 5 M aqueous NaOH, and the resulting mixture was stirred at ambient temperature for 24 h. After evaporation of the solvent, the reaction product was extracted with THF, dried over $MgSO_4$, filtered, and then evaporated under reduced pressure. The residue was purified by column chromatography using 5% MeOH/$CH_3Cl$ containing 1% triethylamine as eluent to afford the desired product **L1** (0.345 g, 37%).

*Coumaric Acid–Lipoamine Conjugate (**3-L1**).* To a solution of **L1** in dry DMF (10 mL) were added the *trans* coumaric acids **3** (104.8 mg, 0.40 mmol) and 1-ethyl-3-(3-dimethylaminopropyl)carbodiimide hydrochloride (EDC; 93.9 mg, 0.49 mmol) in 3 mL of DMF, and the mixture was stirred at 4 °C for 10 min. After the addition of DMAP (6.1 mg, 0.05 mmol) and 1-hydroxybenzotriazole (HOBt; 75.0 mg, 0.49 mmol), the resulting mixture was stirred under $N_2$ atmosphere at 4 °C for 1 h, and then at 25 °C for 18 h. After evaporation of the solvent, products dissolved in chloroform were washed with saturated $NaHCO_3$, saturated citric acid, and brine, successively. Organic layer was dried over $MgSO_4$, filtered, and then

**Scheme 1. Synthesis of Coumaric Acid 3′**

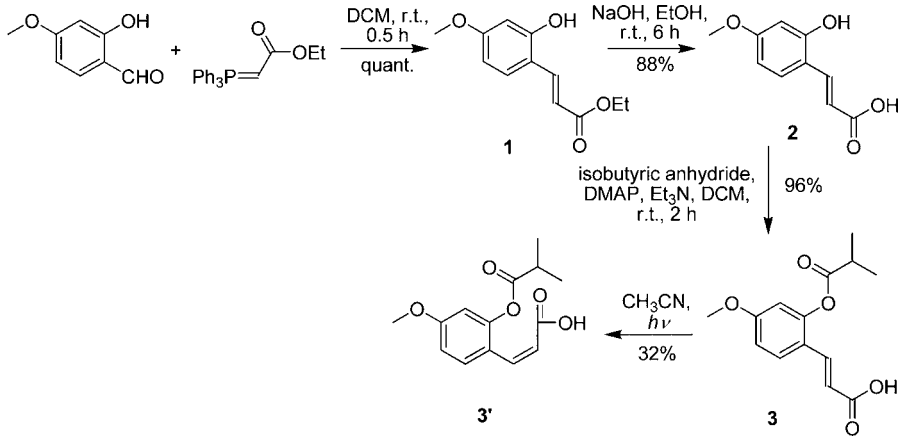


evaporated under reduced pressure. The residue was purified by column chromatography using hexane/ethyl acetate (3:2) as eluent to afford the desired product **3-L1** as a white solid (55.7 mg, 31.4%): $^1$H NMR (300 MHz, $CDCl_3$) $\delta$ 7.63 (d, $J$ = 8.8 Hz, 1H), 7.63 (d, $J$ = 15.5 Hz, 1H), 6.77 (dd, $J$ = 2.4, 8.6 Hz, 1H), 6.59 (d, $J$ = 2.6 Hz, 1H), 6.22 (d, $J$ = 15.5, 1H), 5.54 (br, 1H), 3.79 (s, 3H), 3.54 (m, 1H), 3.34 (q, 2H), 3.12 (m, 2H), 2.87 (m, 1H), 2.44 (m, 1H), 1.89 (m, 1H), 1.68 (br, 4H), 1.4–1.5 (m, 4H), 1.35 (d, $J$ = 7.0 Hz, 6H); $^{13}$C NMR (75 MHz, $CDCl_3$) $\delta$ 175.3, 165.8, 161.4, 150.5, 133.9, 127.6, 120.2, 120.1, 112.7, 108.0, 56.2, 55.5, 40.2, 39.5, 38.4, 34.8, 34.2, 29.5, 28.9, 26.7, 19.0; HRMS (FAB+) $m/z$: Calcd for $C_{22}H_{31}NO_4S_2$: 438.1773 $[M+H]^+$, found 438.1785 $[M+H]^+$.

*Coumaric Acid–Lipoamine Conjugate (3′-L1).* A chloroform solution (15 mL) of **3-L1** (39.3 mg, 0.09 mmol) in a quartz glass vial was exposed to UV light (312 nm) at ambient temperature for 0.5 h. Evaporation of the solvent gave the corresponding *cis* isomer **3′-L1** as a white solid (quant.): $^1$H NMR (270 MHz, $CDCl_3$) $\delta$ 7.17 (d, $J$ = 8.4 Hz, 1H), 6.69 (dd, $J$ = 2.5, 8.6 Hz, 1H), 6.55 (d, $J$ = 11.9 Hz, 1H), 6.50 (d, $J$ = 2.5 Hz, 1H), 6.15 (br, 1H), 5.97 (d, $J$ = 11.9, 1H), 3.75 (s, 3H), 3.44 (m, 1H), 3.09 (m, 2H), 3.02 (q, 2H), 2.75 (m, 1H), 2.37 (m, 1H), 1.81 (m, 1H), 1.71 (br, 4H), 1.4–1.5 (br, 4H), 1.24 (d, $J$ = 6.8 Hz, 6H); $^{13}$C NMR (67.5 MHz, $CDCl_3$) $\delta$ 176.3, 167.0, 160.8, 149.1, 130.9, 130.0, 128.7, 122.3, 112.1, 107.4, 56.5, 55.6, 40.2, 39.0, 38.4, 34.7, 34.1, 28.9, 28.7, 26.4, 19.0; HRMS (FAB+) $m/z$: Calcd for $C_{22}H_{31}NO_4S_2$: 438.1773 $[M+H]^+$, found 438.1773 $[M+H]^+$.

**Synthesis of GNRs.** GNRs were synthesized by the photochemical method reported by Niidome et al.[48] with a slight modification. To an aqueous solution (12 mL) of $HAuCl_4 \cdot 3H_2O$ (2 mM, Aldrich) and cetyltrimethylammonium bromide (CTAB, 80 mM) were added cyclohexanone (100 $\mu$L), 0.15 M $AgNO_3$ (50 $\mu$L), and 80 mM ascorbic acid (400 $\mu$L). The resulting colorless solution was exposed to UV light ($\lambda$ = 250–400 nm) at ambient temperature for 40 min. The resulting dark solution was purified by repeating centrifugation at 12,000 rpm (20 min) and washing with water, and then the precipitates containing the CTAB-capped GNRs were suspended in deionized water.

**Preparation of GNR Conjugates.** Typically, amino linkers **L1**–**L4** (20 mM, 200 $\mu$L) were added to a 200 $\mu$L solution of CTAB-coated GNR (0.2–0.6 $\mu$M), which was then incubated at 25 °C for 12–18 h. The GNR solution was then centrifuged (10,000 rpm, 10 min), decanted, and redispersed in water twice to remove excess linkers. Finally, surface-modified GNRs (**L1**–**L4**@GNRs) were resuspended in 200 $\mu$L of deionized water. To the GNR solution were added *cis* coumaric acids (**3′** or **6′**, 8 $\mu$mol) and EDC (10 $\mu$mol) in 200 $\mu$L of DMF or acetonitrile and the mixture was stirred at 4 °C for 10 min. DMAP (1 $\mu$mol) and HOBt (10 $\mu$mol) were added to the mixture and stirred at 4 °C for 1 h, and then at 25 °C for 12–18 h. The mixture was centrifuged, decanted, and redispersed in DMF–$H_2O$ (1:1) to remove unconjugated coumaric acids. The GNR conjugates thus obtained were finally resuspended in 200 $\mu$L of deionized water. Conjugation of the coumaric acids to the surface of GNRs was confirmed by $^1$H NNR (Supporting Information).

*Transmission Electron Microscopy (TEM).* A drop of the nanoparticle solution was allowed to air-dry onto an elastic-carbon-coated copper grid (ELS-C10, Okenshoji, Japan). TEM images were obtained with a JEOL JEM-1400 electron microscope operating at an accelerating voltage of 120 kV.

**Zeta Potential Measurement.** Zeta potentials of the surface modified GNRs were measured with a Malvern Nano-ZS Zetasizer in disposable cuvettes. GNPs either in ethanol or in water were sonicated before each measurement. Measurements were carried out in triplicate, and the Smoluchowski approximation was used to convert the electrophoretic mobility to zeta potential.

**Porcine Liver Esterase (PLE)-Catalyzed Hydrolysis.** Purified PLE (carboxylic-ester hydrolase; EC 3.1.1.1; E-2884) was obtained from Sigma as a suspension in a 3.2 M $(NH_4)_2SO_4$ solution (pH 8). The suspension containing 1 × $10^4$ units of PLE was diluted to 0.7 mL with phosphate buffer (0.05 M, pH 7.4) containing 2% DMSO. Then, 140 $\mu$L of the prepared GNR conjugates (0.1–0.2 $\mu$M) was combined with the above-mentioned buffer–PLE solution in a quartz cuvette. During the reaction, the cuvette was incubated at 37 °C and subjected to fluorescence measurement.

**DNA Binding Assay.** For preparation of the hydrolysate of **3′-L3**@GNR, the conjugates were incubated at pH 10 for 1 h, neutralized, and then centrifuged at 10,000 rpm for 15 min. Then, 1 $\mu$g of plasmid DNA (ΦX174 RF I, New England Biolabs) was added to 5 $\mu$L of the GNR conjugates (**3′-L3**@GNRs, hydrolyzed **3′-L3**@GNRs, or **L3**@GNRs, 3 nM) and incubated at ambient temperature for 30 min. The solution was diluted with 400 $\mu$L of 1.27 $\mu$M ethidium bromide (EB, Nippon Gene) containing 20% DMF and subjected to fluorescence measurement.


dx.doi.org/10.1021/bc3005599 | *Bioconjugate Chem.* 2013, 24, 1435–1444

**Scheme 2. Synthesis of Coumaric Acid 6′**

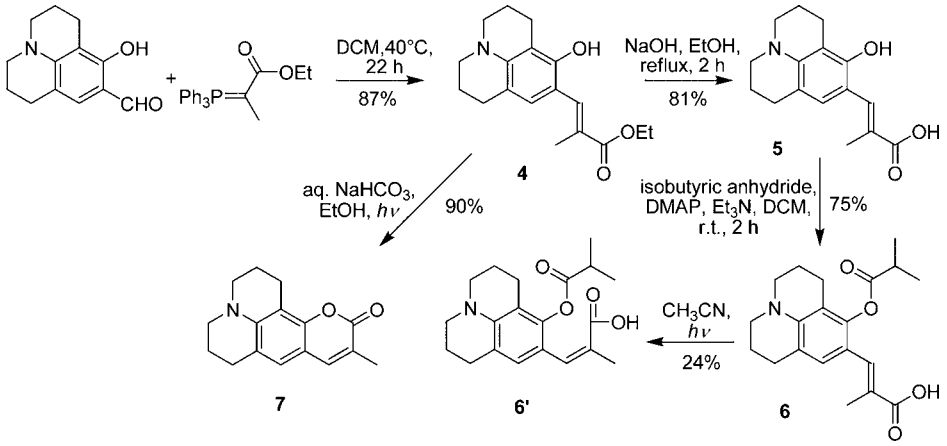


**Bovine Serum Albumin (BSA) Binding Assay.** Gold nanoparticles (**3′-L3**@GNR or hydrolyzed **3′-L3**@GNR, 0.03 nM) in PBS buffer (pH 7.0) containing 5% DMSO were incubated with various concentrations (0.02−0.30 wt %) of BSA (SIGMA, A4378) for 10 min at ambient temperature. Absorption spectra were recorded in the wavelength range of 400−900 nm.

**Cell Culture and Fluorescence Imaging.** Human lung cancer cells A549 (American Type Culture Collection) were cultured in Dulbecco's Modified Eagle Medium supplemented with 10% fetal bovine serum and 1% penicillin/streptomycin at 37 °C in a humidified incubator with an atmosphere containing 5% $CO_2$. Cells were plated in 96-well imaging microplates ($5 \times 10^3$ cells/well) and incubated for 24 h. Various concentrations of GNR conjugates were added to the medium. The cells were further incubated for 1−24 h, washed with fresh PBS buffer three times, and then observed with a Keyence BZ-8100 fluorescence microscope using appropriate excitation and emission filters. The fluorescence intensity was determined with a Promega GloMax multi microplate reader ($\lambda_{ex}$ = 365 nm, $\lambda_{em}$ = 410−460 nm).

## RESULTS AND DISCUSSION

**Design and Synthesis of GNR Conjugates.** Esterase-sensitive coumaric acid structures for protecting amino groups on the surface of GNRs were synthesized according to the reaction pathways shown in Schemes 1 and 2. It has been reported that photoisomerization of the *trans* coumaric acids gives the corresponding *cis* isomers in acceptable yields.[34] Therefore, we first attempted to protect the phenol hydroxyl group of *o*-coumaric acids and then converted them into the *cis* isomers by UV irradiation. As starting materials, we chose two commercially available salicylic aldehyde derivatives, 8-hydroxyjulolidine-9-carboxaldehyde and 2-hydroxy-4-methoxybenzaldehyde. Wittig olefination of the aldehydes with triphenylphosphorane in $CH_2Cl_2$ and the following alkali hydrolysis gave the corresponding carboxylic acids **2** and **5** in good yields.[43,44] We first attempted acetylation of the phenol hydroxyl group of **2** to obtain the corresponding acetyl esters. Photoisomerization of the resulting carboxylic acid in acetonitrile was performed with a UV light source (312 nm) until the *trans* to *cis* isomer conversion reached ∼70%, and then the generated *cis* isomer was purified by HPLC. However, the *cis* isomer possessing the acetyl group was thermally hydrolyzed and transformed into 7-methoxycoumain during the purification. Thus, the phenol hydroxyl groups of **2** and **5** were protected with the isobutyryl group by reaction with isobutyric anhydride; the carboxylic acids **3** and **6** were obtained and were further converted to the *cis* isomers **3′** and **6′** by UV irradiation. The *cis* isomers **3′** and **6′** were stable at −20 °C for at least a few months.

GNRs were prepared by the photochemical method following the previously reported procedures with minor modifications.[48,49] Typically, the aqueous solution of Au(III) ions containing AgCl, CTAB, acetone, and cyclohexanone was treated with ascorbic acid, and the resulting colorless Au(I) solution was then exposed to UV light through a cutoff filter ($\lambda$ = 240−400 nm) at room temperature. Replacing cyclohexane, which was used in the original studies, with cyclohexanone increased the reproducibility of the results. The dark-purple solution was centrifuged and GNRs were collected as the precipitate. Dispersion of GNRs in aqueous buffer solution showed the characteristic plasmon absorption band at around 700 nm. Transmission electron microscope analysis of the synthesized GNRs suggested their particle size was (36 ± 4) × (11 ± 2) nm (aspect ratio 3.3 ± 0.4).

The surface of GNRs is easily modified by conjugation with thiol compounds (**L1−4**) via the Au−S bond (Figure 2). To avoid potential aggregation of GNRs during the assays, the GNR surfaces were modified with heterobifunctional PEG having a thiol group on one terminus and an amino group on the other end (**L2−4**) for covalent attachment of the *cis* coumaric acids **3′** and **6′**. It has been demonstrated that PEG coating of the surface of gold nanoparticles enhances biocompatibility and dispersibility in aqueous solution.[50] The CTAB-capped GNRs prepared as above were incubated with **L1** or the PEG linkers **L2−4**, and then further conjugated with **3′** or **6′** in the presence of 1-(3-dimethylaminopropyl)-3-ethylcarbodiimide, DMAP, and 1-hydroxybenzotriazole. Unreacted materials were removed by multiple centrifugation and washing steps until *cis* coumaric acids were not detected in the supernatant solution.

GNRs functionalized with **3′** via lipoamine **L1** linker (**3′-L1@GNR**) were immediately aggregated in aqueous solution. By contrast, the coumaric acid−GNR conjugates possessing PEG linkers (**3′-L2**@GNR, **3′-L3**@GNR, **3′-L4**@GNR, **6′-L3**@GNR, and **6′-L4**@GNR) were dispersed in aqueous buffer solution (pH 7.0) to some extent; in particular, the functional PEG linker **L4** improved their dispersibility. Figure 3 shows the results of TEM observation of the synthesized **3′-L3**@GNR. The apparent size of the surface-modified GNRs as determined


dx.doi.org/10.1021/bc3005599 | *Bioconjugate Chem.* 2013, 24, 1435−1444

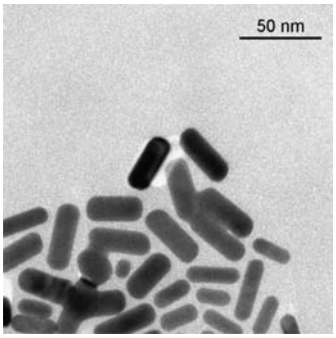


**Figure 3.** Transmission electron microscope image of 3′-**L3**@GNRs.

by transmission electron microscopy ((34 ± 3 nm) × (11 ± 2 nm)) was unchanged from that of unmodified GNRs, because only the gold core is visible at the current acceleration voltage (Supporting Information). The amino-PEG-modified GNRs **L2**−**4**@GNR showed positive surface potentials of +29 to +32 mV; on the other hand, GNRs modified with the coumaric acids showed somewhat neutralized surface potentials of +17 to +22 mV (Table 1). As has been discussed earlier,[51] a small amount of residual CTAB on the surface of GNRs might be attributable to the slightly positive potentials.

**Table 1. Zeta Potential (mV) of the Surface Modified GNRs**

| | end protection | | |
|---|---|---|---|
| nanoparticle | non | 3′ | 6′ |
| **L2**@GNR | +31.6 ± 0.5 | +17.6 ± 2.1 | – |
| **L3**@GNR | +31.4 ± 2.1 | +21.8 ± 1.8 | +17.1 ± 2.6 |
| **L4**@GNR | +29.0 ± 2.1 | +18.3 ± 0.4 | +17.2 ± 0.6 |

**Hydrolysis and Lactonization of the Coumaric Acids on the Surface of GNRs.** To demonstrate enzyme-catalyzed hydrolysis and lactonization of the coumaric acids by esterase, PLE was used for the assays. PLE can recognize and hydrolyze a wide variety of ester structures. Figure 4A shows time-dependent fluorescence spectra obtained from the PLE-treated coumaric acid−lipoamine conjugates (3′-**L1**, 10 $\mu$M) in aqueous phosphate buffer containing 2% DMSO. Depending on the incubation time, emission from the photoexcited 7-methoxycoumarin increased; by contrast, only a slight increase was observed for 3′-**L1** untreated with PLE. The PLE-catalyzed hydrolysis of 3′-**L1** and the appearance of 7-methoxycoumarin were also observed on the HPLC chromatograms (data not shown). The apparent pseudofirst-order rate constant ($k_{obs}$) for the formation of 7-methoxycoumarin from 3′-**L1** was determined to be 3.7 × $10^{-4}$ $s^{-1}$ ($t_{1/2}$ = 32 min), which is comparable to the value for a similar phenyl isobutylate.[33] The formation of coumarin should proceed via the following multistep reactions: (1) recognition of the coumaric acid by PLE, (2) hydrolytic release of the isobutyl group, and (3) lactonization of the coumaric acids and release of the amines. It is thus possible that conjugation of the coumaric acids to the surface of GNRs affects the accessibility of PLE as well as the rate of lactonization.

We next examined PLE-catalyzed hydrolysis of the coumaric acid protecting group on the surface of synthesized GNRs. In the present study, we prepared GNR conjugates having various linker structures (3′-**L2**@GNR, 3′-**L3**@GNR, 3′-**L4**@GNR, 6′-**L3**@GNR, and 6′-**L4**@GNR) to investigate the effects of linker structures and length on PLE sensitivity. As in the case of the

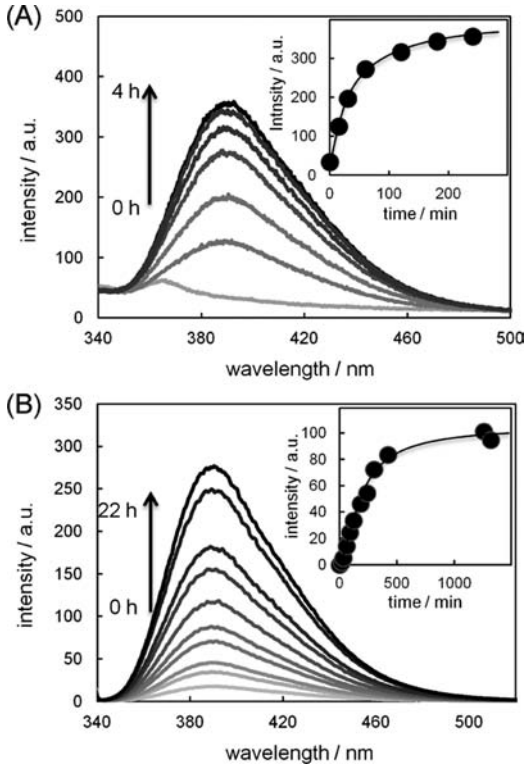


**Figure 4.** Typical fluorescence spectra of (A) 3′-**L1** and (B) 3′-**L3**@GNR after incubation with PLE at 37 °C for the indicated periods. (Insets) Time course of the PLE-catalyzed release of fluorescent coumarins from (A) 3′-**L1** ($\lambda_{ex}$ = 280 nm, $\lambda_{em}$ = 390 nm) and (B) 3′-**L3**@GNR ($\lambda_{ex}$ = 330 nm, $\lambda_{em}$ = 390 nm).

free ligand 3′-**L1**, fluorescent coumarin formation was observed for all of the conjugates, although the dispersibility of the nanoparticles varied (Figure 4B). It has been suggested that gold nanoparticles are quite efficient fluorescence quenchers;[52] however, it is less likely that the emission from the released coumarins is quenched by the GNR conjugates. In a separate experiment, addition of the GNR conjugates to free coumarins in aqueous buffer solutions showed no emission quenching, probably because the surface PEG structures shield the gold core from the free photoexcited coumarins. Table 2 shows

**Table 2. Pseudo-First-Order Kinetic Rate Constants ($k_{obs}$) of the PLE-Catalyzed Release of Coumarin Derivatives from the Surface-Modified GNRs**

| | 3′ | | 6′ | |
|---|---|---|---|---|
| nanoparticle | $k_{obs}/s^{-1}$ | $t_{1/2}$/min | $k_{obs}/s^{-1}$ | $t_{1/2}$/min |
| **L2**@GNR | 4.6 × $10^{-5}$ | 250 | – | – |
| **L3**@GNR | 3.6 × $10^{-5}$ | 320 | 2.4 × $10^{-4}$ | 49 |
| **L4**@GNR | 1.8 × $10^{-4}$ | 65 | 3.4 × $10^{-4}$ | 34 |

kinetic data for the formation of PLE-catalyzed coumarin from the GNR conjugates, as determined from the fluorescence profiles. Under the present experimental conditions, the values of $k_{obs}$ for coumarin formation from 3′-**L4**@GNR and 6′-**L4**@GNR were larger than from 3′-**L2**@GNR, 3′-**L3**@GNR, and 6′-**L3**@GNR. Therefore, dispersibility of the GNR conjugates might affect the accessibility of PLE to coumaric acids on the surface of the GNR conjugates. Also, precursor 6′ is hydrolyzed faster than 3′ suggesting that 6′ is a good substrate for


dx.doi.org/10.1021/bc3005599 | *Bioconjugate Chem.* 2013, 24, 1435−1444

monitoring the conversion process on the surface of the GNR conjugates. Based on the concentration of the GNR conjugates and the fluorescence intensity obtained after completion of the hydrolysis, it can be calculated that approximately $1.8 \times 10^3$ molecules of procoumarin **6′** are tethered on the surface of single **6′-L4**@GNR.

Esterase-catalyzed hydrolysis of the surface structure of the GNR conjugates formed fluorescent coumarins and GNRs with amino-PEG linkers as the counterparts. Alteration of the surface chemical structures of GNRs would change the interactions between nanoparticles and biomolecules in the cells. It has been reported that metal nanoparticles coated with amino-functional chemical structures interact with biomacromolecules, such as DNA and BSA.[16,53] To confirm the formation of amino residues on the surface of the synthesized GNR conjugates, changes in the interactions between plasmid DNA and the prepared GNR conjugates (**3′-L3**@GNR and **6′-L3**@GNR) were monitored using a fluorescent intercalator displacement assay. Positively charged EB is a well-known intercalator toward DNA. Upon intercalation between base pairs in DNA, photoexcited EB shows intense fluorescence and thus competitive binding of the GNRs to the DNA duplex could be monitored as changes in fluorescence intensity.

As shown in Figure 5, addition of **3′-L3**@GNR to ΦX174 plasmid DNA resulted in no changes in the fluorescence spectra

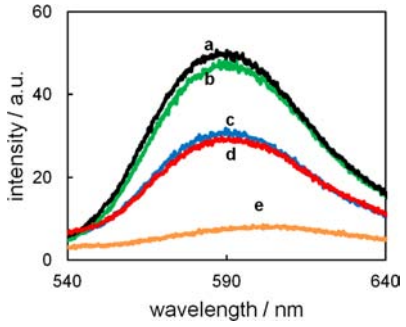


**Figure 5.** Fluorescence spectra of EB in $H_2O$–DMF (4:1) as observed upon excitation at 330 nm. (a) EB, **3′-L3**@GNR, and DNA; (b) EB and DNA; (c) EB, DNA, and **L3**@GNR; (d) EB, DNA, and hydrolyzed **3′-L3**@GNR; (e) EB alone.

of EB. By contrast, hydrolysate of **3′-L3**@GNR suppressed the fluorescence intensity, suggesting that amino-PEG-coated GNRs (**L3**@GNR) generated as a result of the coumarin release interacted with plasmid DNA, and either directly inhibited the intercalation of EB into DNA base pairs or induced conformational changes in the DNA duplex.

We further evaluated the formation of amino groups by examining the affinity of the GNR conjugates to BSA before and after the hydrolytic conversion of the surface. Recent studies have demonstrated protein absorption on the surface of manufactured nanoparticles depending on the size, charge density, and other surface properties. Such binding can change the original surface characteristics of nanoparticles and affect the bioprocesses both inside and outside the living cells. In fact, protein absorption on the surface altered the efficiency of cellular uptake.[16,54−56] UV-absorption spectra ($\lambda$ = 400−900 nm) of the prepared GNR conjugates **3′-L3**@GNR were recorded in the presence of BSA (Figure 6). BSA does not show intense absorption bands in that wavelength range.[57] The absorption bands corresponding to the surface plasmon of

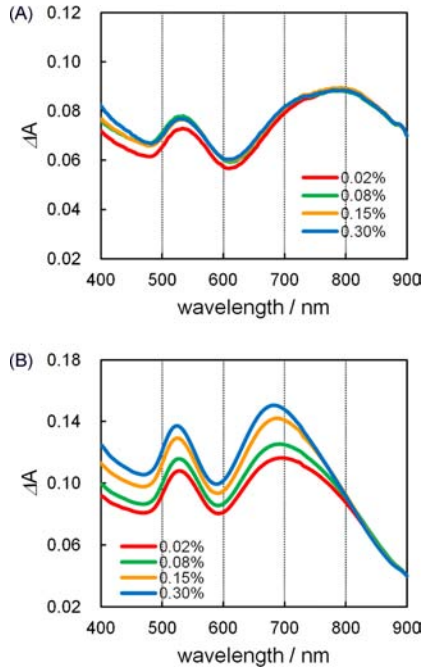


**Figure 6.** UV–vis absorption spectra of GNRs in the presence of various concentrations of BSA (0.02–0.30%). (A) **3′-L3**@GNRs in PBS buffer (pH 7.0) containing 5% DMSO were incubated with BSA. (B) Hydrolyzed **3′-L3**@GNRs were resuspended in PBS buffer (pH 7.0) containing BSA and 5% DMSO. Absorption spectra were normalized at 900 nm.

GNRs were not influenced by the addition of BSA. By contrast, a hypsochromic shift of the surface plasmon band at around 700 nm was observed when BSA was added to the hydrolysate of **3′-L3**@GNR (expected to be converted to **L3**@GNR), implying that the dispersibility of GNRs was changed as a result of surface conversion and the subsequent BSA absorption on the surface. Taken together with the fact that the shape and peak position of the transverse surface plasmon band at around 520 nm were not much affected by the BSA addition, these findings indicate that the Au(111) surface is crucial in the interaction between BSA and **L3**@GNR.[58]

As demonstrated above, we could observe deprotection of amino groups as the formation of fluorescent coumarins. Although DNA and BSA are not easily accessed by the incorporated GNRs in the cells, it is highly likely that such conversion of the surface chemical structures could alter interactions between GNRs and other cytoplasmic proteins and lipids

**Cellular Uptake of GNR Conjugates and Their Surface Structural Changes inside Living Cells.** Previous studies on cellular uptake of nonfluorescent metal nanoparticles were conducted using dark-field microscopy and inductively coupled plasma mass spectroscopy. Dark-field microscopy is useful for directly observing metal nanoparticles within cells without any pretreatment, but scattering light from subcellular organelles sometimes makes quantifying the relative amounts of uptaken nanoparticles difficult. However, inductively coupled plasma mass spectroscopy is capable of detecting metal ion concentration down to the parts-per-billion (ppb) level, and it is thus suited for determining the number of metal nanoparticles within cells, although some adequate pretreatments, such as collection and homogenization of the cells, are necessary prior to measurement. In principle, the GNR


dx.doi.org/10.1021/bc3005599 | Bioconjugate Chem. 2013, 24, 1435−1444

conjugates prepared in this study can form equal amounts of surface-modified nanoparticles and fluorescent coumarin derivatives, and thus relative amounts of nanoparticles with specific surface structures can be estimated based on the fluorescence intensity using fluorescence microscopy.

We first examined the cytotoxicity of the prepared GNRs toward human lung adenocarcinoma epithelial cell line A549 using the WST method.[59] Colorimetric measurements indicated that, after 24 h of incubation, GNR conjugates showed a cell viability of more than 80% (data not shown), suggesting that the prepared nanoparticles could be used for *in vitro* studies. GNR conjugates were incubated with A549 cells and the subsequent coumarin release was observed with a fluorescence microscope. We first examined **3′-L3**@GNR to demonstrate the surface conversion; however, excitation of the nanoparticles with short-wavelength light illumination resulted in cell death under the microscope during the observation. A newly synthesized coumarin derivative **7** absorbs UV-light in the wavelength range of 300−460 nm, and shows fluorescence between 450 and 600 nm (Supporting Information). Therefore, **6′-L4**@GNR was employed as an alternative, and the microscopic images were obtained through a filter (460 nm ± 25 nm) by excitation at 360 nm ± 20 nm (Figure 7). A549

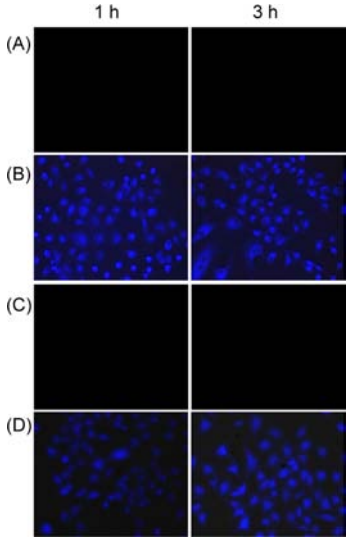


**Figure 7.** Fluorescence microscope images of A549 cells incubated with (A) no additive, (B) coumarin **7** (1.0 $\mu$M), (C) **L4**@GNRs (1.1 nM), or (D) **6′-L4**@GNRs (0.8 nM) for the indicated periods. Cultured cells were photoexcited at 360 ± 20 nm, and the fluorescence images were obtained in the wavelength range of 460 ± 25 nm.

cells treated with **6′-L4**@GNR showed intense blue fluorescence after a short period of incubation (~0.5 h) and the fluorescence from within the cells lasted over 6 h. By contrast, when the coumarin derivative **7** was added to the cells, intense blue fluorescence from within the cells was observed only a few minutes after the addition. Also, when **6′-L4**@GNR was treated with the medium buffer, no increase of fluorescence was observed (data not shown). The time-dependent surface conversion of **6′-L4**@GNR in A549 cells was monitored as the formation of **7** by quantifying fluorescence intensity from A549 cells cultured in 96-well imaging plates for desired periods of time (Figure 8). These data imply that amino-PEG-coated nanorods (**L4**@GNRs) were increasingly formed after 6 h under the present conditions, most likely in endosomes or

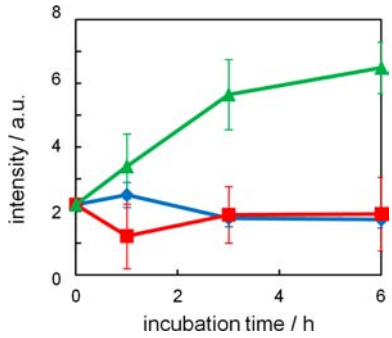


**Figure 8.** Quantification of fluorescence intensity (410−460 nm) upon excitation at 365 nm. A549 cells were incubated (●) alone or in the presence of either (■) **L4**@GNRs or (▲) **6′-L4**@GNRs (0.8 nM, respectively) for the indicated periods.

lysosomes. From the time profiles of fluorescence intensity in Figure 8, concentration of coumarin **7** released after 3 h incubation was calculated to be 0.12 $\mu$M, which implies that 8% of **6′** on the surface of **6′-L4**@GNR were hydrolyzed and the same amount of amine residues were generated. According to a previous report, GNRs are internalized into A549 cells and transferred to endosomes and lysosomes over several hours.[60] Therefore, the rate-determining cellular uptake process should be responsible for the observed slow release of coumarins. Direct quantification of GNRs in living cells based on fluorescence intensity is generally difficult, because the quantum efficiency of such nanorods has been reported to be very low,[61] limiting the widespread use of the fluorescence properties of GNRs in biosensing. Unfortunately, the enzyme-catalyzed surface structure conversion and the concomitant release of fluorophore seemed to be slower than we expected. In view of the fact that $k_{obs}$ for the release of coumarin from free **3′-L1** is larger than those from GNR conjugates, it might be possible to enhance the reactivity by designing a linker with appropriate length.

We envision that the present approach would be applicable for determining relative amounts of surface-modified gold nanoparticles in living cells based on the fluorescence intensity of the released coumarins. For example, it would be possible to quantitatively investigate the effects of surface structures of nanoparticles on the excretion from various types of cells based on our strategy.

## ■ CONCLUSIONS

We prepared gold nanoparticles whose surface was modified with esterase-sensitive coumaric acids and evaluated the PLE-catalyzed surface structure conversion of the particles accompanied by the formation of fluorescent coumarins as reporter molecules. PEG-coated GNRs protected by **6′** (**6′-L4**@GNR) were used for the cell assay, because of their stability in aqueous media and ease of observation with a fluorescence microscope, and we successfully observed the time-dependent surface conversion. This approach might provide a potential strategy for investigating the effects of surface chemical structures of nanoparticles on processes of excretion from within the cells. Another application of our nanoparticles would be for delivering nanoscale drugs into cells even when the surfaces are unfavorably charged for internalization. Alteration of the surface polarity could change the interaction between nanoparticles and biomolecules, resulting in the nanoparticles being accumulated in the cells and


dx.doi.org/10.1021/bc3005599 | *Bioconjugate Chem.* 2013, 24, 1435−1444

enhancing antitumor effects. As we are interested in the effects of the surface chemical structure on the exocytotic pathways of the metal nanoparticles, we are currently investigating the fate of gold nanoparticles after the surface conversion based on this approach.

## ■ ASSOCIATED CONTENT

### Supporting Information

$^1$H NMR spectra of the conjugates, TEM micrograph, UV-absorption and fluorescence spectra of **7**, UV-absorption maxima of the GNR conjugates. This material is available free of charge via the Internet at http://pubs.acs.org.

## ■ AUTHOR INFORMATION


### Corresponding Author

*Phone: +81-75-383-7054. Fax: +81-75-383-2504. E-mail: takeoit@scl.kyoto-u.ac.jp.


### Notes

The authors declare no competing financial interest.

## ■ ACKNOWLEDGMENTS

The authors appreciate the measurement of FAB mass spectra by Mr. Hiroshi Hatta, Kyoto University. This work was supported by Hosokawa Powder Technology Foundation and the Program for Fostering Regional Innovation "Kyoto Environmental Nanotechnology Cluster" administered by the Ministry of Education, Culture, Sports, Science, and Technology (MEXT), Japan.

## ■ ABBREVIATIONS

GNR, gold nanorod; CTAB, cetyltrimethylammonium bromide; EB, ethidium bromide; EDC, 1-ethyl-3-(3-dimethylaminopropyl)carbodiimide hydrochloride; HOBt, 1-hydroxybenzotriazole; DMAP, 4-dimethylaminopyridine

## ■ REFERENCES


(1) Niemeyer, C. M. (2001) Nanoparticles, proteins, and nucleic acids: biotechnology meets materials science. *Angew. Chem., Int. Ed. 40*, 4128−4158.

(2) Katz, E., and Willner, I. (2004) Integrated nanoparticle−biomolecule hybrid systems: synthesis, properties, and applications. *Angew. Chem., Int. Ed. 43*, 6042−6108.

(3) Michalet, X., Pinaud, F. F., Bentolila, L. A., Tsay, J. M., Doose, S., Li, J. J., Sundaresan, G., Wu, A. M., Gambhir, S. S., and Weiss, S. (2005) Quantum dots for live cells, in vivo imaging, and diagnostics. *Science 307*, 538−544.

(4) Rosi, N. L., and Mirkin, C. A. (2005) Nanostructures in biodiagnostics. *Chem. Rev. 105*, 1547−1562.

(5) Kim, C., Agasti, S. S., Zhu, Z., Isaacs, L., and Rotello, V. M. (2010) Recognition-mediated activation of therapeutic gold nanoparticles inside living cells. *Nat. Chem. 2*, 962−966.

(6) Kim, B., Han, G., Toley, B. J., Kim, C. −K., Rotello, V. M., and Forbes, N. S. (2010) Tuning payload delivery in tumour cylindroids using gold nanoparticles. *Nat. Nanotechnol. 5*, 467−472.

(7) Saha, K., Agasti, S. S., Kim, C., Li, X., and Rotello, V. M. (2012) Gold nanoparticles in chemical and biological sensing. *Chem. Rev. 112*, 2739−2779.

(8) Li, C., Hu, J., Liu, T., and Liu, S. (2011) Stimuli-triggered off/on switchable complexation between a novel type of charge-generation polymer (CGP) and gold nanoparticles for the sensitive colorimetric detection of hydrogen peroxide and glucose. *Macromolecules 44*, 429−431.

(9) Li, C., Wu, T., Hong, C., Zhang, G., and Liu, S. (2012) A general strategy to construct fluorogenic probes from charge-generation polymers (CGPs) and AIE-active fluorogens through triggered complexation. *Angew. Chem., Int. Ed. 51*, 455−459.

(10) Ge, Z. and Liu, S. (2013) Functional block copolymer assemblies responsive to tumor and intracellular microenvironments for site-specific drug delivery and enhanced imaging performance. *Chem. Soc. Rev.* In press. (DOI: 10.1039/C3CS60048C)

(11) Murphy, C. J., Gole, A. M., Stone, J. W., Sisco, P. N., Alkilany, A. M., Goldsmith, E. C., and Baxter, S. C. (2008) Gold nanoparticles in biology: beyond toxicity to cellular imaging. *Acc. Chem. Res. 41*, 1721−1730.

(12) Lewinski, N., Colvin, V., and Drezek, R. (2008) Cytotoxicity of nanoparticles. *Small 4*, 26−49.

(13) Lee, S. H., Bae, K. H., Kim, S. H., Lee, K. R., and Park, T. G. (2008) Amine-functionalized gold nanoparticles as non-cytotoxic and efficient intracellular siRNA delivery carriers. *Int. J. Pharm. 364*, 94−101.

(14) Alkilany, A. M., and Murphy, C. J. (2010) Toxicity and cellular uptake of gold nanoparticles: what we have learned so far? *J. Nanopart. Res. 12*, 2313−2333.

(15) Leroueil, P. R., Hong, S., Mecke, A., Baker, J. R., Jr., Orr, B. G., and Holl, M. M. B. (2007) Nanoparticle interaction with biological membranes: does nanotechnology present a Janus face? *Acc. Chem. Res. 40*, 335−342.

(16) Lynch, I., and Dawson, K. A. (2008) Protein-nanoparticle interactions. *Nano Today 3*, 40−47.

(17) Chen, J., Hessler, J. A., Putchakayala, K., Panama, B. K., Khan, D. P., Hong, S., Mullen, D. G., DiMaggio, S. C., Som, A., Tew, G. N., Lopatin, A. N., Baker, J. R., Jr., Holl, M. M. B., and Orr, B. G. (2009) Cationic nanoparticles induce nanoscale disruption in living cell plasma membranes. *J. Phys. Chem. B 113*, 11179−11185.

(18) Mukhopadhyay, A., Grabinski, C., Nabiul Afrooz, A. R. M., Saleh, N. B., and Hussain, S. (2012) Effect of gold nanosphere surface chemistry on protein adsorption and cell uptake in vitro. *Appl. Biochem. Biotechnol. 167*, 327−337.

(19) Goodman, G. M., McCusker, C. D., Yilmaz, T., and Rotello, V. M. (2004) Toxicity of gold nanoparticles functionalized with cationic and anionic side chains. *Bioconjugate Chem. 15*, 897−900.

(20) Arvizo, R. R., Miranda, O. R., Thompson, M. A., Pabelick, C. M., Bhattacharya, R., Robertson, D., Rotello, V. M., Prakash, Y. S., and Mukherjee, P. (2010) Effect of nanoparticle surface charge at the plasma membrane and beyond. *Nano Lett. 10*, 2543−2548.

(21) Lin, J., Zhang, H., Chen, Z., and Zheng, Y. (2010) Penetration of lipid membranes by gold nanoparticles: insights into cellular uptake, cytotoxicity, and their relationship. *ACS Nano 4*, 5421−5429.

(22) Jiang, Y., Hu, X., Hu, J., Liu, H., Zhong, H., and Liu, S. (2011) Reactive fluorescence turn-on probes for fluoride ions in purely aqueous media fabricated from functionalized responsive block copolymers. *Macromolecules 44*, 8780−8790.

(23) Jiang, X., Dausend, J., Hafner, M., Musyanovych, A., Röcker, C., Landfester, K., Mailänder, V., and Nienhaus, G. U. (2010) Specific effects of surface amines on polystyrene nanoparticles in their interactions with mesenchymal stem cells. *Biomacromolecules 11*, 748−753.

(24) Zhao, F., Zhao, Y., Liu, Y., Chang, X., Chen, C., and Zhao, Y. (2011) Cellular uptake, intracellular trafficking, and cytotoxicity of nanomaterials. *Small 7*, 1322−1337.

(25) Wilhelm, C., Billotey, C., Roger, J., Pons, J. N., Bacri, J.-C., and Gazeau, F. (2003) Intracellular uptake of anionic superparamagnetic nanoparticles as a function of their surface coating. *Biomaterials 24*, 1001−1011.

(26) Jahn, M. R., Nawroth, T., Fütterer, S., Wolfrum, U., Kolb, U., and Langguth, P. (2012) Iron oxide/hydroxide nanoparticles with negatively charged shells show increased uptake in Caco-2 cells. *Mol. Pharmaceutics 9*, 1628−1637.

(27) Teow, Y., Asharani, P. V., Handec, M. P., and Valiyaveettil, S. (2011) Health impact and safety of engineered nanomaterials. *Chem. Commun.*, 7025−7038.

(28) Chithrani, B. D., and Chan, W. C. W. (2007) Elucidating the mechanism of cellular uptake and removal of protein-coated gold nanoparticles of different sizes and shapes. *Nano Lett. 7*, 1542−1550.
(29) Jin, H., Heller, D. A., and Strano, M. S. (2008) Single-particle tracking of endocytosis and exocytosis of single-walled carbon nanotubes in NIH-3T3 cells. *Nano Lett. 8*, 1577−1585.
(30) Slowing, I. I., Vivero-Escoto, J. −L., Zhao, Y., Kandel, K., Peeraphatdit, C., Trewyn, B. G., and Lin, V. S.−Y. (2011) Exocytosis of mesoporous silica nanoparticles from mammalian cells: from asymmetric cell-to-cell transfer to protein harvesting. *Small 7*, 1526−1532.
(31) Yanes, R. E., Tarn, D., Hwang, A. A., Ferris, D. P., Sherman, S. P., Thomas, C. R., Lu, J., Pyle, A. D., Zink, J. I., and Tamanoi, F. (2013) Involvement of lysosomal exocytosis in the excretion of mesoporous silica nanoparticles and enhancement of the drug delivery effect by exocytosis inhibition. *Small 9*, 697−704.
(32) Shan, D., Nicolaou, M. G., Borchardt, R. T., and Wang, B. (1997) Prodrug strategies based on intramolecular cyclization reactions. *J. Pharm. Sci. 86*, 765−767.
(33) Wang, B., Zhang, H., Zheng, A., and Wang, W. (1998) Coumarin-based prodrugs. part 3: structural effects on the release kinetics of esterase-sensitive prodrugs of amines. *Bioorg. Med. Chem. 6*, 417−426.
(34) Zheng, A., Wang, W., Zhang, H., and Wang, B. (1999) Two new improved approaches to the synthesis of coumarin-based prodrugs. *Tetrahedron 55*, 4237−4254.
(35) Liao, Y., Hendrata, S., Yong, S., and Wang, B. (2000) The effect of phenyl substituents on the release rate of esterase-sensitive coumarin-based prodrugs. *Chem. Pharm. Bull. 48*, 1138−1147.
(36) Amsberry, K. L., and Borchardt, R. T. (1991) Amine prodrugs which utilize hydroxy amide lactonization. I. A potential redox-sensitive amide prodrug. *Pharm. Res. 8*, 323−330.
(37) Gomes, P., Vale, N., and Moreira, R. (2007) Cyclization-activated prodrugs. *Molecules 12*, 2484−2506.
(38) Liu, R., Aw, J., Teo, W., Padmanabhan, P., and Xing, B. (2010) Novel trimethyl lock based enzyme switch for the self-assembly and disassembly of gold nanoparticles. *New J. Chem. 34*, 594−598.
(39) Cho, H., Bae, J., Garripelli, V. K., Anderson, J. M., Jun, H. −W., and Jo, S. (2012) Redox-sensitive polymeric nanoparticles for drug delivery. *Chem. Commun. 48*, 6043−6045.
(40) Dubertret, B., Calame, M., and Libchaber, A. J. (2001) Single-mismatch detection using gold-quenched fluorescent oligonucleotides. *Nat. Biotechnol. 19*, 365−370.
(41) Dulkeith, E., Morteani, A. C., Niedereichholz, T., Klar, T. A., and Feldmann, J. (2002) Fluorescence quenching of dye molecules near gold nanoparticles: radiative and nonradiative effects. *Phys. Rev. Lett. 89*, 203002.
(42) Yun, C. S., Javier, A., Jennings, T., Fisher, M., Hira, S., Peterson, S., Hopkins, B., Reich, N. O., and Strouse, G. F. (2005) Nanometal surface energy transfer in optical rulers, breaking the FRET barrier. *J. Am. Chem. Soc. 127*, 3115−3119.
(43) Bunce, R. A., and Schilling, C. L., III (1997) Five- and six-membered lactones and lactams by tandem dealkoxycarbonylation-Michael addition reactions. *Tetrahedron 53*, 9477−9486.
(44) Das, S. K., Dinda, S. K., and Panda, G. (2009) Enantioselective synthesis of functionalized 1-benzoxepines by phenoxide ion mediated 7-endo-tet carbocyclization of cyclic sulfates. *Eur. J. Org. Chem.*, 204−207.
(45) Shiono, H., and Noda, H. Jpn. Kokai Tokkyo Koho JP 09227560 A, September 2, 1997.
(46) Maus, L., Dick, O., Bading, H., Spatz, J. P., and Fiammengo, R. (2010) Conjugation of peptides to the passivation shell of gold nanoparticles for targeting of cell-surface receptors. *ACS Nano 4*, 6617−6628.
(47) Morita, T., Kimura, S., and Kobayashi, S. (2000) Photocurrent generation under a large dipole moment formed by self-assembled monolayers of helical peptides having an *N*-ethylcarbazolyl group. *J. Am. Chem. Soc. 122*, 2850−2859.
(48) Niidome, Y., Nishioka, K., Kawasaki, H., and Yamada, S. (2003) Rapid synthesis of gold nanorods by the combination of chemical reduction and photoirradiation processes; morphological changes depending on the growing processes. *Chem. Commun.*, 2376−2377.
(49) Kim, F., Song, J. H., and Yang, P. (2002) Photochemical synthesis of gold nanorods. *J. Am. Chem. Soc. 124*, 14316−14317.
(50) Tshikhudo, T. R., Wang, Z., and Brust, M. (2004) Biocompatible gold nanoparticles. *Mater. Sci. Technol. 20*, 980−984.
(51) Vigderman, L., Manna, P., and Zubarev, E. R. (2012) Quantitative replacement of cetyl trimethylammonium bromide by cationic thiol ligands on the surface of gold nanorods and their extremely large uptake by cancer cells. *Angew. Chem., Int. Ed. 51*, 636−641.
(52) Fan, C., Wang, S., Hong, J. W., Bazan, G. C., Plaxco, K. W., and Heeger, A. J. (2003) Beyond superquenching: hyper-efficient energy transfer from conjugated polymers to gold nanoparticles. *Proc. Natl. Acad. Sci. U. S. A. 100*, 6297−301.
(53) Prado-Gotor, R., and Grueso, E. (2011) A kinetic study of the interaction of DNA with gold nanoparticles:mechanistic aspects of the interaction. *Phys. Chem. Chem. Phys. 13*, 1479−1489.
(54) Kaufman, E. D., Belyea, J., Johnson, M. C., Nicholson, Z. M., Ricks, J. L., Shah, P. K., Bayless, M., Pettersson, T., Feldotö, Z., Blomberg, E., Claesson, P., and Franzen, S. (2007) Probing protein adsorption onto mercaptoundecanoic acid stabilized gold nanoparticles and surfaces by quartz crystal microbalance and $\zeta$-potential measurements. *Langmuir 23*, 6053−6062.
(55) Ravindran, A., Singh, A., Raichur, A. M., Chandrasekaran, N., and Mukherjee, A. (2010) Studies on interaction of colloidal Ag nanoparticles with bovine serum albumin (BSA). *Colloids Surf. B Biointerfaces 76*, 32−37.
(56) Baier, G., Costa, C., Zeller, A., Baumann, D., Sayer, C., Araujo, P. H. H., Mailänder, V., Musyanovych, A., and Landfester, K. (2011) BSA adsorption on differently charged polystyrene nanoparticles using isothermal titration calorimetry and the influence on cellular uptake. *Macromol. Biosci. 11*, 628−638.
(57) Pan, B., Cui, D., Xu, P., Li, Q., Huang, T., He, R., and Gao, F. (2007) Study on interaction between gold nanorod and bovine serum albumin. *Colloids Surf., A: Physicochem. Eng. Aspects 295*, 217−222.
(58) Chakraborty, S., Joshi, P., Shanker, V., Ansari, Z. A., Singh, S. P., and Chakrabarti, P. (2011) Contrasting effect of gold nanoparticles and nanorods with different surface modifications on the structure and activity of bovine serum albumin. *Langmuir 27*, 7722−7731.
(59) Ishiyama, M., Shiga, M., Sasamoto, K., Mizoguchi, M., and He, P. (1993) A new sulfonated tetrazolium salt that produces a highly water-soluble formazan dye. *Chem. Pharm. Bull. 41*, 1118−1122.
(60) Wang, L., Liu, Y., Li, W., Jiang, X., Ji, Y., Wu, X., Xu, L., Qiu, Y., Zhao, K., Wei, T., Li, Y., Zhao, Y., and Chen, C. (2011) Selective targeting of gold nanorods at the mitochondria of cancer cells: implications for cancer therapy. *Nano Lett. 11*, 772−780.
(61) Mohamed, M. B., Volkov, V., Link, S., and El-Sayed, M. A. (2000) The 'lightning' gold nanorods: fluorescence enhancement of over a million compared to the gold metal. *Chem. Phys. Lett. 317*, 517−523.